

A Simultaneous Spectroscopic Measurement of the Global and Edge Local Structures in the Ion Temperature and Plasma Rotation Profiles in the Compact Helical System

Shin NISHIMURA, Ken-ichi NAGAOKA, Yasuo YOSHIMURA, Kiichiro NAKAMURA, Harukazu IGUCHI, Tsuyoshi AKIYAMA, Takashi MINAMI, Tetsutaro OISHI, Katsumi IDA, Kazuo TOI, Akihiro SHIMIZU, Mitsutaka ISOBE, Chihiro SUZUKI, Chihiro TAKAHASHI, Shoichi OKAMURA, Keisuke MATSUOKA and CHS Group

National Institute for Fusion Science, 322-6 Oroshi-cho, Toki 509-5292, Japan

(Received 8 February 2007 / Accepted 27 April 2007)

In charge exchange spectroscopy (CXS), a simultaneous observation in different plasma toroidal cross sections and/or viewing ports is required to investigate radial distributions of ion temperatures $T_i(r)$, and poloidal rotation velocities $V_p(r)$ in magnetically confined toroidal plasmas. In recent studies of the edge transport barrier (ETB) in the Compact Helical System (CHS), a simultaneous viewing of the vertically elongated and the horizontally elongated plasma cross sections is used to improve the spatial resolution at the edge region. The 90 fibers used for this purpose are connected to one spectrometer, and a 256×243 pixel sampling CCD is used to detect the diffraction image. It is found that there is a localized edge ion temperature pedestal region with $\Delta T_i \approx 100$ eV and $\Delta r/a \approx 0.1$, where r and a are flux surface averaged minor radii of measured surfaces and the outermost flux surface, respectively. The negative radial electric field at the edge is increased in the high confinement phase because of the increased ion pressure.

© 2007 The Japan Society of Plasma Science and Nuclear Fusion Research

Keywords: visible spectroscopy, non-symmetric toroidal configuration, plasma transport, improved confinement, transport barrier

DOI: 10.1585/pfr.2.037

1. Introduction

In studies of magnetically confined toroidal plasmas, detailed radial distributions of plasma parameters are required, and thus various multi-channel measurement techniques are used. Modern charge exchange spectroscopic (CXS) diagnostics used [1] to measure ion temperatures and plasma rotations (flows along the magnetic flux surfaces), often employ 2 dimensional CCD detectors to observe charge exchange excited spectral lines at several tens of points in real space simultaneously [2]. In helical and/or stellarator devices without axisymmetry, the radial range and the spatial resolution depend on the toroidal location of the diagnostic. In the so-called high-confinement mode (H mode) with edge transport barriers (ETB) which was actively studied in various tokamaks in 1990's, the importance of the poloidal rotation in the edge barrier region is widely recognized [3]. In contrast to tokamaks, the edge poloidal flows have not been studied in detail in helical devices even though some phenomena exhibiting a "transition" of the H_α line intensity in the peripheral region were observed. Instead of the edge poloidal flows, the effect of radial electric field shear in the internal thermal transport barrier in the Compact Helical System (CHS) was studied [4, 5]. After these studies, another spontaneous tran-

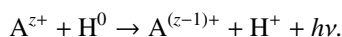
sition phenomenon accompanying the reduction of the H_α line intensity was found in the CHS with an increased heating power by two neutral beams [6]. A newly found similarity to the tokamak H-mode is a threshold for the neutral beam injection (NBI) power [7]. However, there are still quantitative and qualitative differences between the "H-mode" with the ETB in the CHS and that in the tokamaks. The role of plasma flows and/or radial electric fields in the ETB plasmas in the CHS remains as an important open issue. In contrast to tokamak H-mode plasmas, the radial electric field estimated by the poloidal flow velocity of the impurity ions in the core region, $r/a < 0.9$, is a weak negative one (a few kV/m [8]) corresponding to so-called ion-root defined in the neoclassical theory [9]. Here, r and a ($= 0.2$ m) are flux surface averaged minor radii of measured surfaces and the outermost flux surface, respectively. These previous CXS measurements were done by a vertical viewing at a vertically elongated plasma cross section. This selection of the viewing chord put a priority on the measured range in the real space and did not put it on the spatial resolution. Since the cross sections of the flux surfaces are helically rotating ellipses with a long/short radii ratio of about 2 in heliotron devices such as the CHS and the Large Helical Device (LHD) [10], vertically and horizontally elongated cross sections must be

author's e-mail: nishimura.shin@lhd.nifs.ac.jp

chosen depending on purposes of studies. Recently, from various edge plasma measurements in ETB plasmas in the CHS, it is suggested that the edge pedestal region, where the ion pressure gradients and a corresponding ion flow are expected, is very narrow (for e.g., $\Delta r/a \approx 0.05$) if it exists [6]. Radial profiles of the flow velocities and the ion temperatures in such a narrow region could not be detected with the previous CXS geometry at a vertically elongated section [11] with the chord spacing $\Delta R = 7.5$ mm in a major radial direction corresponding to a spatial resolution of $\Delta r/a \approx 0.06$. Even though a vertical view at horizontally elongated sections subtends a limited radial range, it has superior spatial resolution near the edge region. The chord spacing $\Delta R = 6.3$ mm at the equatorial plane corresponds to a spatial resolution of $\Delta r/a \approx 0.02$. In this paper, we report measurements from CXS at both vertically and horizontally elongated sections.

2. Charge Exchange Spectroscopic Measurement

The CXS [1, 2] uses the following reactions between fully ionized light impurity ions A^{z+} , where z is the charge of the ion, and the externally injected neutral hydrogen beam (H^0) to measure the velocity distribution (the flow velocity and the temperature) of the A^{z+} ions:



This spectral line emission is caused only in the beam path and therefore the ion velocity distribution in the core region is directly obtained from the Doppler shift and broadening of the lines. The fully ionized carbon C^{6+} as the impurity ion A^{z+} and an emitted CVI line of $\Delta n = 8-7$ and $\lambda = 5290 \text{ \AA}$ are often used [1, 2]. The poloidal rotation in the tokamak H-mode was detected by this method. Spectral lines from the neutral hydrogen in the visible range are easily excited by electron impacts in the peripheral region, and this spontaneous emission from the region without the neutral beam obscures the charge exchange emission from the core region inside of the outermost flux surface. This difficulty of direct measurements using hydrogen spectral lines for the proton distribution function is one reason to use impurity ions, in spite of a fact that our purpose is to study the distribution function of proton (or deuterium, tritium ions) as the working gas of the experiments. Especially in studies of radial electric fields, note that we do not measure directly the dominant ion component of the plasmas. We can know not only the flow velocity and the temperature of the impurity ion, but also the impurity density profile from the intensity of the charge exchange excited lines [11]. In the study of the transition phenomenon in the ETB plasmas, however, we must consider the density profile of the proton and thus the impurity density profile is out of scope of this paper. In Sec. 4, we will use the edge electron density profile obtained by a lithium beam probe (LiBP) method [12].

Here we consider on some technical problems, which are peculiar to the medium sized helical devices such as the CHS. In the CHS, the typical ion temperature is a few hundred eV and a typical flow velocity of the C^{6+} ions is a few km/s. There are several problems causing apparent wavelength shifts which make it difficult to measure the plasma flow velocities of this order: (1) mechanical wavelength offset of the spectrometers ($\Delta\lambda \sim 0.5 \text{ \AA}$), (2) aberration of spectrometers ($\Delta\lambda \sim 0.1 \text{ \AA}$), (3) horizontal displacements of the fibers at the entrance slits ($\Delta\lambda \sim 0.01 \text{ \AA}$), and (4) the spectral fine structure of hydrogen-like ions [1]. These problems were not described in Ref. [1], which assumed applications to large tokamaks with ion temperatures of $T_i \geq 2 \text{ keV}$ and toroidal rotations of $V_t \approx 100 \text{ km/s}$. The best approach to measure correctly the Doppler shifts by canceling the mechanical wavelength offset is with bidirectional viewing (simultaneous views along opposite viewing directions) [10, 11, 13]. Therefore, in the multi-channel CXS systems to measure the plasma rotation profiles, the required number of observing channels includes not only that for observing the beam from one direction, but also that for the other direction to detect the absolute value of the Doppler shifts, as well as channels for measuring the background radiation [2]. Here, the ‘‘background’’ radiation means the emission caused without beams as mentioned above. Even though this background emission for the case of the impurity lines is relatively small compared with the case of the hydrogen lines, the spectral components due to this process must be subtracted because they distort the line shape and affect the measurements of both the temperature and flow velocity. For this purpose, the additional viewing chords at another section looking off the beams are used (it should be mentioned whether these have essentially identical viewing geometry) [2]. In the present study to investigate the edge local structure simultaneously, we used fibers of 24 ch \times 3 ports for the global profile at the vertically elongated sections. The vertically viewing chords of 9 ch \times 2 ports at the horizontally elongated sections are added to resolve the plasma edge region. Two tangentially injected heating neutral hydrogen beams are used for this diagnostic. One (40 keV) is used for the vertically elongated section, and the other one (30 keV) is used for the horizontally elongated section. The location of the vertically viewing chords at the vertically elongated cross section is illustrated in Refs. [11] and [14]. At this location, the beam radius (half-width at half-maximum \sim 6 cm in the vertical direction) can be neglected compared with the plasma size in the vertical direction (minor radius of \sim 30 cm). Figure 1 shows the outermost flux surface and the vertically viewing chords at the horizontally elongated sections. Since available ports for these sections are limited in this experimental term, the sections with (without) the beam are observed by viewing from upper (lower) side only. This outboard edge of the horizontally elongated section is nearer to the beam focus point than the vertically elongated section and thus the beam diameter is about half

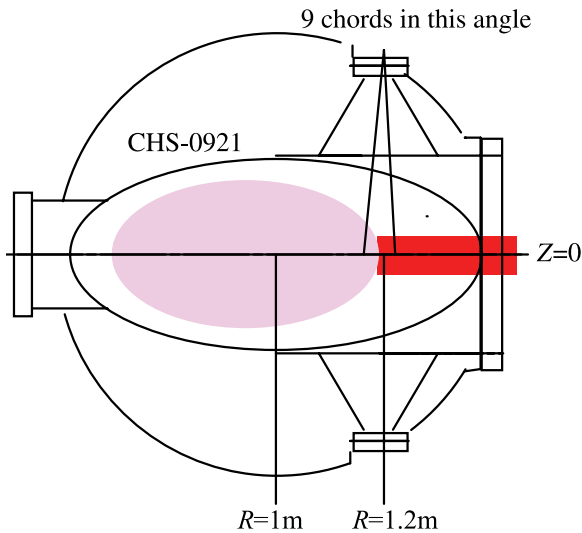


Fig. 1 Geometrical location of the outermost flux surface and the vertically viewing chords in the vacuum vessel at the horizontally elongated sections.

of that at the vertically elongated section. Therefore beam radius is negligible also at this horizontally elongated section measurement. The Doppler shifts at all of these chords are calculated as deviations from the “standard” wavelength (without Doppler shifts) obtained by the bidirectional viewing of the beam [11]. Therefore, total number of fiber channels that one Czerny-Turner type spectrometer (with a focal length of 1 m and a 2400 l/mm grating) has to detect simultaneously is 90. The diffraction image is detected by a 256×243 pixels sampling CCD with an image intensifier (effective image size is $11.6 \text{ mm} \times 8.7 \text{ mm}$). The apparent wavelength shifts due to the distortion of the diffraction image caused by the aberration and the fiber displacements were calibrated with a mercury lamp. The Doppler shifts are calculated from a non-linear least-squares fitting of the superposition of Doppler broadened fine structural line components since the red-side/blue-side asymmetric splitting of the spectral line of the CVI line ($\Delta\lambda \approx 1 \text{ \AA}$) is not negligible compared with the Doppler broadening and the Doppler shift in typical CHS plasmas with ion temperatures of $T_i \approx 0.2 \text{ keV}$ and poloidal flow velocities of $V_p < 10 \text{ km/s}$.

3. Global Radial Profiles in the ETB Plasmas

Figure 2 shows time traces of plasma global parameters showing the spontaneous transition to the state with the ETB. The two neutral beams are injected into a low-density hydrogen plasma created by 200 kW of electron cyclotron heating (ECH) at 53 GHz. The maximum port-through neutral beam power is 800 kW for each. The magnetic configuration used in this example has a vacuum magnetic axis position of $R_{ax} = 0.92 \text{ m}$ and a quadrupole

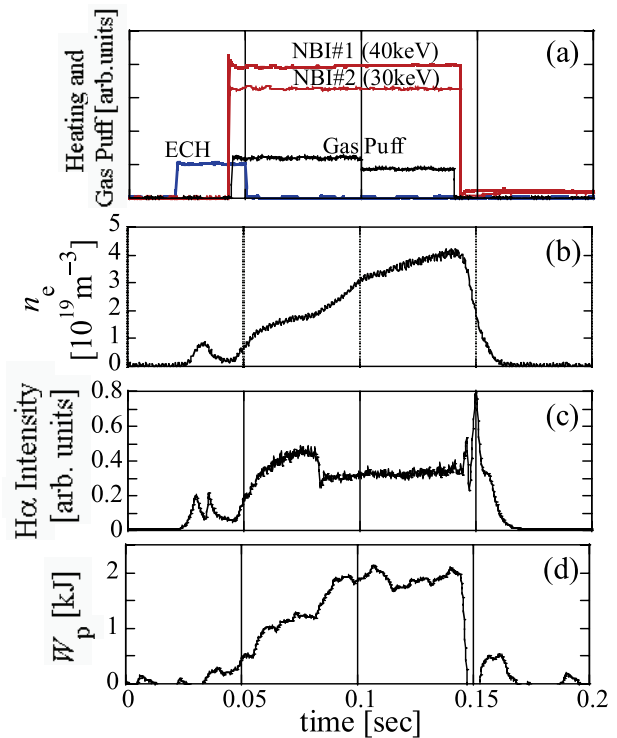


Fig. 2 Time traces of parameters in a discharge with ETB formation: (a) time sequences of ECH, NBI, and gas puffing; (b) line averaged electron density; (c) H_α emission; (d) diamagnetic energy.

magnetic field of $B_q = 0$. The magnetic field strength is $B = 0.95 \text{ T}$ at the magnetic axis. The electron temperature and density profiles are measured with a 24 channel Thomson scattering system and a laser interferometer. The line averaged electron density is controlled by gas puffing to keep a slow raise up to $4 \times 10^{19} \text{ m}^{-3}$. At $t = 80 \text{ ms}$, a spontaneous low-confinement(L) / high-confinement(H) transition appears in the plasma edge region, which is shown by the drop of H_α intensity. The radial profiles of the temperature and the density are shown in Fig. 3. The ion temperature profile given by the CXS at the vertically elongated section is also shown there. In these figures for results at the equatorial plane $Z = 0$, we show also positions of magnetic axis $r/a = 0$ and the outermost flux surface $r/a = 1$ of the finite beta equilibrium calculation assumed in the LiBP measurement described in the next section. The density profile given by the Thomson scattering show that the edge density starts to increase making a broader profile. Although broader density profiles with flat or hollow structures at the center region of $r/a \leq 0.6$ have been often observed in previous various types of discharges in helical/stellarator devices [4, 5, 11], the density in the ETB plasmas after the drop of the H_α intensity becomes especially high near the edge $r/a \approx 1$ [6, 7]. The electron and ion temperatures are kept almost constant before and after the transition. Therefore the diamagnetic plasma energy increases as well by 50% due to the increase of the

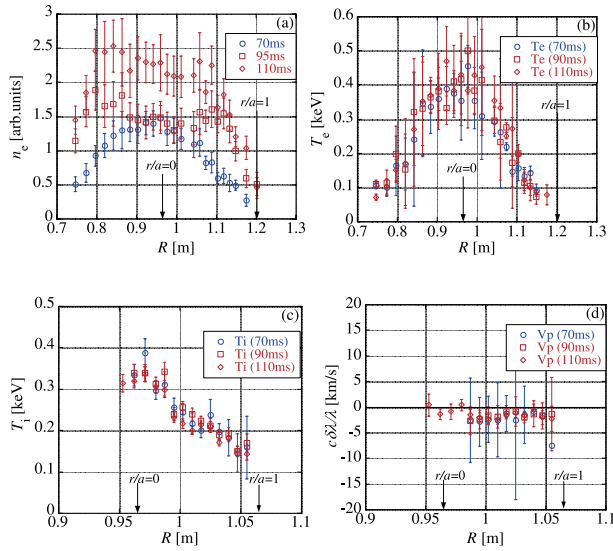


Fig. 3 Radial distribution profiles of : (a), (b) the electron density and temperature given by the Thomson scattering at a horizontally elongated section; (c), (d) ion temperature and the Doppler shift of the CVI line $\delta\lambda$ giving the poloidal flow velocity by $V_p = c\delta\lambda/\lambda$ at the vertically elongated sections.

density. Since the electron density (n_e) and the ion temperature (T_i) profiles in the core region in the ETB phase are rather flat ($\partial T_i/\partial r \approx 200 \text{ eV}/0.2 \text{ m}$), ion pressure given by $p_i = n_i T_i$, where $n_i \approx n_e$ is the density of proton, also has only a small radial gradient $\partial p_i/\partial r$ in the core region and has a localized large radial gradient at the edge region. Figure 3 (d) shows the poloidal flow velocity of C^{6+} ions (V_p) measured by a vertically viewing at the vertically elongated cross section of the plasmas. It is already known that the V_p is dominated by the $\mathbf{E} \times \mathbf{B}$ drift in the radial force balance for the C^{6+} ions since diamagnetic drifts of impurities with the α_z scaling are small compared with the $\mathbf{E} \times \mathbf{B}$ drift [11]. Therefore, hereafter, we interpret the V_p as the radial electric fields E_r by a relation $E_r \approx V_p B$. The collisionality in this operational condition corresponds to the plateau regime defined in the neoclassical transport theory. Since the E_r in the plateau regime in non-symmetric toroidal plasmas is determined mainly by the bulk ion pressure gradient $E_r \approx (1/en_i)\partial p_i/\partial r$ [9], the V_p is determined by the pressure gradient of the protons. Therefore the measured V_p is relatively small in the core region because of the small proton pressure gradient $\partial p_i/\partial r$. Except for the strong positive radial electric field of $E_r \approx +10 \text{ kV/m}$ in low-collisionality operations [15] such as the N-ITB case, this type of weak negative E_r of a few kV/m is a typical in the high density operations with NBI in CHS [11].

4. Edge Local Structure

Figure 4 shows the edge local structure obtained by the CXS at the horizontally elongated section. The ion

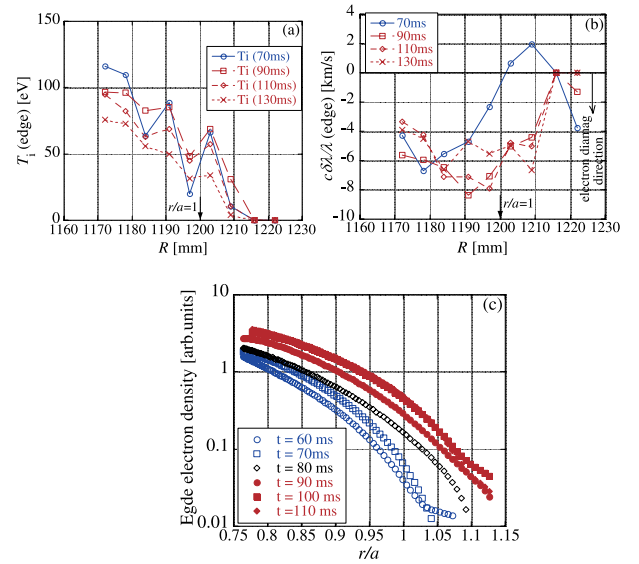


Fig. 4 (a): The ion temperature T_i , and (b): the flow velocity by $V_p = c\delta\lambda/\lambda$ near the LCFS at $R \cong 1.2 \text{ m}$. (c): The edge electron density obtained by the LiBP. A width of $\Delta r/a = 0.1$ corresponds to that of $\Delta R \cong 2.5 \text{ cm}$ at the equatorial plane $Z = 0$.

temperature profile has a pedestal region with $\Delta T_i \approx 100 \text{ eV}$ near the edge at $R = 1.2 \text{ m}$ and does not show clear changes after the L/H transition timing $t = 80 \text{ ms}$. It is consistent with previous measurements at the vertically elongated section indicating that the edge ion temperature is about $T_i \approx 100 \text{ eV}$ and does not clearly change at the transition. However, the plasma density in this region is increasing in this transition phase. The V_p at the edge is in the direction of the electron diamagnetic drift and shows a change corresponding to this growth. As mentioned above, we have to investigate the proton pressure $n_i T_i \approx n_e T_i$ instead of that of the C^{6+} ions at this edge pedestal region. Here we use the edge electron density (n_e) profile given by the lithium beam probe [12] for this purpose. In this diagnostic technique, the electron impact excited line emission from the lithium beam is used to investigate the electron density profile at the edge region where the Thomson scattering method is not effective because of the low electron temperature. Figure 4 (c) shows this edge electron density profile. Although this diagnostic also measures the density at the outboard edge as described in Ref. [12], intersections of the lithium beam and the chords do not locate at the equatorial plane $Z = 0$. To compare this result with the other measurement results at $Z = 0$, we show in Fig. 4 (c) the measured density as a function of normalized and flux surface averaged minor radius r/a by assuming a finite beta equilibrium that approximately reproduces the Shafranov shift in the measured electron temperature profile. Here, it should be noted that the Shafranov shifts in NBI heated plasmas in the CHS are often affected by fast-ion pressure. Therefore it is better to interpret shifts of measured tem-

perature profiles as the actual Shafranov shifts [14]. Note, however, also that the shapes and positions of the flux surfaces near the outermost surface are insensitive to these finite beta effects, especially in inward shifted limiter configurations (using the vacuum vessel wall at the inboard side of the vertically elongated section as the limiter) in which the L/H transition has been observed [6, 7]. A density gradient region, where $\partial(\ln n_e)/\partial r$ is large, clearly moves outward by $\Delta r/a \approx 0.1$ after the transition. Following the aforementioned characteristics of the Shafranov shifts in the CHS, and by a fact that the measured electron and ion temperatures in Figs. 3 (b), 3 (c), and 4 (a) do not change after the L/H transition, it can be understood that this “shift” of the edge density profile is not due to that of the magnetic flux surfaces. This change of the density gradient in $(1/n_i)\partial p_i/\partial r = T_i\partial(\ln n_i)/\partial r + \partial T_i/\partial r$ induces a change in the radial electric field. The flux surface averaged electric field strength of $E_r \equiv -\partial\phi/\partial r \approx 10$ kV/m at the low temperature region of $T_i \leq 100$ eV is strong in view of its associated poloidal Mach number [16] and will be an important key in considering the transition mechanisms. Since the flux surface averaged poloidal magnetic field strength in this edge region is $B_p \approx 0.18$ T, the Mach number $M_p \equiv E_r/(B_p v_T)$, where v_T is the thermal velocity, for protons at a radial position of $T_i \approx 50$ eV ($v_T \approx 1 \times 10^5$ m/s) and $E_r \approx 10$ kV/m is $M_p \approx 0.6$. In this electric field strength range, the neoclassical viscosity becomes a non-linear function of the radial electric field, and this non-linearity is one of explanations for the transition phenomena [3, 16].

5. Conclusion

The ion temperatures $T_i(r)$, poloidal flow velocities $V_p(r)$ of C^{6+} ions are investigated using a simultaneous observation in different plasma toroidal cross sections. The vertical viewings at the vertically elongated cross sections with the 24 chords \times 2 directions and at the horizontally elongated section with 9 chords are used for the global and the edge local structures, respectively. In NBI heating operation with the ETB formation, it was found that the edge poloidal flow indicating the strong negative radial electric field of $E_r \approx -10$ kV/m is formed after the L/H transition at the ion temperature pedestal region of $T_i < 100$ eV and $\Delta r/a \approx 0.1$. The ion pressure gradient region near the edge moves outward by $\Delta r/a \approx 0.1$ and the measured poloidal flow velocity corresponds to this change of the pressure gradient. The poloidal Mach number for the protons is order of unity after the L/H transition since the radial electric field strength becomes large in the low ion temperature region. These behaviors of the E_r in the spontaneous transition are qualitatively similar to those in the tokamak H-mode.

The N-ITB formation [4, 5] was previously investi-

gated by using an applied E_r control operating at low density ($0.4 \times 10^{19} \text{ m}^{-3}$) and applying ECH of $P_{\text{ECH}} \sim 200$ kW. By making the collisionality low we obtain the “electron-root” condition defined in the neoclassical theory [4, 15]. In contrast to this, the most important characteristic of the ETB [6, 7] is its spontaneous formation in high-density plasmas. Since this transition occurs in plasmas with sufficient particle fueling by the neutral beams and gas puffing, the subsequent density increase raises the pressure after the transition. In spite of these large differences, increases of pressures accompanying formations of strong E_r are obtained in both of the improved modes. Another observation in this spontaneous L/H transition was that the region with the E_r shear and the pressure gradients shifted outward after the transition. Therefore suppressions of fluctuations in the ETB operation will not be so simple, when comparing with the previous comparison of the fluctuations in states with and without the E_r shear in the N-ITB operation [4]. If there is an “improved” layer where the fluctuation is suppressed, it will move outward after the transition, and thus the fluctuation measured at a fixed position in the core region may sometimes increase after the transition [6]. This increase of the fluctuation, however, does not conflict with previously established understandings for the turbulent transport [3, 4]. The result obtained in the present study will be useful also in future analyses for results of multi-point fluctuation measurements using Langmuir probes and so on.

Acknowledgement

This work is supported by a NIFS coordinated research program NIFS88KZPD001. One author (S.N.) also thanks Dr. D.R. Mikkelsen for the critical reading of the manuscript.

- [1] R.J. Fonck *et al.*, Phys. Rev. A **29**, 3288 (1984).
- [2] K. Ida and S. Hidekuma, Rev. Sci. Instrum. **60**, 867 (1989).
- [3] ITER Physics Expert Group, Nucl. Fusion **39**, 2175 (1999).
- [4] A. Fujisawa *et al.*, Phys. Rev. Lett. **82**, 2669 (1999).
- [5] T. Minami *et al.*, Nucl. Fusion **44**, 342 (2004).
- [6] S. Okamura *et al.*, Nucl. Fusion **45**, 863 (2005).
- [7] T. Akiyama, S. Okamura, T. Minami *et al.*, Plasma Phys. Control. Fusion **48**, 1683 (2006).
- [8] S. Nishimura *et al.*, Ann. Rep of NIFS 2005 p.271, p.272.
- [9] K.C. Shaing *et al.*, Phys. Fluids **29**, 521 (1986); H. Sugama and W. Horton, Phys. Plasmas **3**, 304 (1996).
- [10] K. Ida *et al.*, Rev. Sci. Instrum. **71**, 2360 (2000).
- [11] S. Nishimura *et al.*, Phys. Plasmas **7**, 437 (2000).
- [12] K. Nakamura *et al.*, Rev. Sci. Instrum. **76**, 013504 (2005).
- [13] A.R. Field, G. Fussmann *et al.*, Nucl. Fusion **32**, 1191 (1992).
- [14] H. Yamada, K. Ida *et al.*, Nucl. Fusion **32**, 25 (1992).
- [15] S. Nishimura *et al.*, Fusion Sci. Technol. **46**, 77 (2004).
- [16] K.C. Shaing, Phys. Fluids **B5**, 3841 (1993).